

Article

# Multi-Factor Coupling Analysis of Porous Leakage in Underwater Gas Pipelines

Hong Ji <sup>1,2,3,\*</sup>, Jie Guo <sup>1,2,3</sup>, Gao Zhang <sup>4</sup>, Ke Yang <sup>1,2,3</sup>, Juncheng Jiang <sup>1,2,3</sup>, Yaxin Wang <sup>4</sup>, Zhixiang Xing <sup>1,2,3,\*</sup> and Haipu Bi <sup>1</sup>

<sup>1</sup> School of Safety Science and Engineering, Changzhou University, Changzhou 213164, China

<sup>2</sup> School of Emergency Management Science and Engineering, Changzhou University, Changzhou 213164, China

<sup>3</sup> Institute of Public Safety and Emergency Management, Changzhou University, Changzhou 213164, China

<sup>4</sup> School of Petroleum Engineering, Changzhou University, Changzhou 213016, China; wyx961009@icloud.com (Y.W.)

\* Correspondence: jihong@cczu.edu.cn (H.J.); xingzhixiang@cczu.edu.cn (Z.X.)

**Abstract:** Natural gas pipeline leaks under the sea will have a significant negative effect on the marine ecosystem, result in significant financial losses, and possibly even harm marine floating objects. The VOF (Volume of Fluid) multi-phase flow model is used to numerically simulate and study the diffusion process of porous leakage in submarine gas pipelines. Experiments confirmed the model's correctness and dependability. Based on this, the coupling effect and the porous effect of the leakage velocity, the size of the leaked pore, and water velocity of the natural gas pipelines on the diffusion of porous leakage in the submarine gas pipelines are analyzed with the test scheme designed by the orthogonal test method. The similarity principle is used to connect the leakage model with the actual application. The results show that three factors, namely, the leakage velocity, the size of leaked pore, and the water velocity, influence the shape of the air mass, the time when the gas reaches the sea surface, and the diffusion range. The size of the leakage hole and the leakage velocity have a substantial impact on the form of the air mass and the amount of time it takes for the gas to reach the sea surface, while the water velocity has no effect. Additionally, while there is essentially little impact from the leakage velocity, the size of the leaky pore and the water velocity have a significant impact on the diffusion range. Furthermore, the porous effect between leaky pores has a significant impact on the gas diffusion range. This study can serve as a guide for risk assessment and emergency decision-making regarding a submarine gas pipeline leak.

**Keywords:** underwater gas pipeline; porous leakage; physical model experiment; numerical simulation; multi-factor coupling analysis; similar principles



**Citation:** Ji, H.; Guo, J.; Zhang, G.; Yang, K.; Jiang, J.; Wang, Y.; Xing, Z.; Bi, H. Multi-Factor Coupling Analysis of Porous Leakage in Underwater Gas Pipelines. *Processes* **2023**, *11*, 1259. <https://doi.org/10.3390/pr11041259>

Academic Editor: Vladimir S. Arutyunov

Received: 25 March 2023

Revised: 15 April 2023

Accepted: 16 April 2023

Published: 19 April 2023



**Copyright:** © 2023 by the authors. Licensee MDPI, Basel, Switzerland. This article is an open access article distributed under the terms and conditions of the Creative Commons Attribution (CC BY) license (<https://creativecommons.org/licenses/by/4.0/>).

## 1. Introduction

Since the 21st century, with the rapid development of the global economy, people's demand for energy has been increasing [1,2]. As a result, people's demand for natural gas continues to increase, and submarine pipelines play an irreplaceable role in the natural gas transportation process [3]. However, due to the harsh subsea environment, submarine natural gas pipelines have long been affected by current erosion [4] and landslides, and pipelines are prone to corrosion and perforation. The impact of human factors such as ship anchoring and fishing vessel operations will also cause leakage of subsea gas pipelines [5–8]. Leakage from a submarine pipeline will harm the regular exploitation of oil and gas reserves, result in significant financial losses, and even have an impact on people's everyday lives [9–11]. In September 2022, a pipeline leak at Russia's Nord Stream gas pipeline resulted in the discharge of about 220,000 tons of methane into the atmosphere, seriously endangering the local ecosystem and hastening global warming [12,13]. If natural gas spreads to the sea, it may be ignited accidentally to cause fires and explosions, which

directly threaten people's lives and property [14,15]. The study of the porous leak diffusion law of subsea gas pipelines can provide appropriate guidance for risk prevention and the establishment of emergency responses.

In recent years, many scholars have conducted much research on submarine pipeline leakage and made great contributions. Initially, underwater gas release experiments were conducted at Statoil's Research Center in Norway to investigate the bubble plume [16]. In 2000, a deep-water experiment was also conducted in Norwegian waters to study the phenomenon of deep-water blowouts, known as DeepSpill [17]. With the development of Computational Fluid Dynamics (CFD) [18–20], a simulation concept which was demonstrated by the DeepSpill experiment was presented to forecast oil and gas blowouts [21]. The diffusion behavior of natural gas leaked from submarine pipelines on the free surface of seawater can be calculated by the coupling Volume of Fluid (VOF) [22,23] and discrete phase model (DPM) in CFD [24]. Meanwhile, this approach was also used to predict the gas distribution through the ocean surface [25] and the resulting surface flows [26]. A Eulerian–Lagrangian CFD model [27] was presented to study the effect of gas dissolution on sea gas release. This model also can be used to study the plume characteristics of downward leakage of underwater pipelines [28]. Wu et al. [29] evaluated the four approaches, which were used to model the release of sea gas by comparing the CFD results with experimental data. Sun et al. [30] studied the significant effects of water depth, velocity and leakage rate on underwater gas migration. The above studies always analyze the model of underwater diffusion. Similar analyses can be seen in other investigations [31–33]. Wang et al. [34] has built a model that can be used to study the formation and breakdown of gas hydrates, which could help to understand the fate of bubbles released in the deep ocean. Li et al. [35] established a CFD model to simulate underwater natural gas leakage and studied the migration and diffusion of natural gas under the influence of the leak hole angle and the river velocity after a leak across a river pipeline. Zhang et al. [36] studied the leakage flow and diffusion behavior of underwater natural gas through experiments. A VOF model was used to study the impact of shock waves caused by leaks in subsea gas pipelines [37]. Mocellin et al. [38] proposed a reliable multiphase discharge model, which is suitable for matching all expected CO<sub>2</sub> emission mechanisms. It was found that the length, inner diameter, and orifice size of the pipeline, as well as other factors, are all somewhat influenced by the gas release duration of the pipeline. Four different conditions can affect gas diffusion under water. These include the leakage diameters, the leakage directions, ocean current velocities, and line pressures [39–41]. These four conditions also affect the height of water leaving the surface and the safety of offshore platforms [42]. In addition, water depth also affects underwater leak characteristics and surface diffusion [43].

The research studies mentioned above are predicated on the idea of single hole leakage. Therefore, the study ignores the impact of porous leakage dispersion on the overall leakage process, the actual leakage process that frequently takes place concurrently. The aim of this study is to construct an experimental methodology for dynamic simulation research using the VOF Euler multiphase flow model and an orthogonal test approach. For the purposes of managing leakage risk and making emergency decisions, multi-factor coupling analysis and porous impact analysis of porous leakage and diffusion of undersea gas pipes provide the necessary technological support.

## 2. Numerical Model

### *Governing Equations*

Gas diffusion in liquid, a two-phase mixed flow that blends gas and liquid, is what causes underwater pipeline leakage. The Volume of Fluid (VOF) model is a multi-phase Euler flow model that is very accurate and trustworthy for simulating flow issues involving two-phase incompatible fluids [24]. The equation is shown in (1)–(4), where  $\alpha$  is the phase fraction,  $\alpha = 0$  represents the first phase (such as air),  $\alpha = 1$  represents the second phase (such as water),  $0 < \alpha < 1$  represents the phase interface, and  $f_\sigma$  is the surface tension.

The VOF model equation is:

$$\rho = \alpha\rho_{water} + (1 - \alpha)\rho_{air} \quad (1)$$

$$\mu = \alpha\mu_{water} + (1 - \alpha)\mu_{air} \quad (2)$$

$$\frac{\partial(\rho u)}{\partial t} + \nabla \cdot (\alpha u) = 0 \quad (3)$$

$$\frac{\partial(\rho u)}{\partial t} + \nabla \cdot (\rho u u) = -\nabla \cdot p + \nabla \cdot T + \rho g + f_{\sigma} \quad (4)$$

The VOF model is used in dynamic modeling to examine the dispersion of porous pipeline leakage. The diffusion process of fluid leakage generally follows the continuity equation, momentum conservation, and energy conservation equations:

$$\frac{\partial \rho}{\partial t} + \frac{\partial}{\partial x_i}(\rho u_i) = 0 \quad (5)$$

where  $x_i$  and  $u_i$  are the  $x$  direction and gas velocity in the  $x$  direction, respectively, and  $\rho$  and  $t$  are the gas density and time, respectively.

The momentum conservation equation is as follows:

$$\frac{\partial}{\partial t}(\rho u_i) + \frac{\partial}{\partial x_j}(\rho u_i u_j) + \frac{\partial p}{\partial x_i} - \frac{\partial \tau_{ij}}{\partial x_j} - \frac{\partial \tau_{ij}^{-1}}{\partial x_j} = 0 \quad (6)$$

in which  $x_j$  is the  $y$  direction,  $u_i$  and  $u_j$  are the gas velocity in the  $x$  direction and the gas velocity in the  $y$  direction, respectively,  $p$  is the gas pressure, and  $\tau_{ij}$  is the component of the viscous stress  $\tau$  acting on the element surface.

The energy conservation equation is as follows:

$$\frac{\partial}{\partial t}(\rho E) + \frac{\partial}{\partial x_j}(\rho u_i E + u_j p) - \frac{\partial}{\partial x_j}(u_i \tau_{ij} + u_i \tau_{ij}^{-1}) + \frac{\partial}{\partial x_j}(q_j + q_j^{-1}) = 0 \quad (7)$$

where  $E$  is the total energy of fluid elements and  $q_j$  is the heat flux in the  $y$  direction.

When the control equation is solved, the SIMPLEC algorithm is adopted for the pressure-velocity coupling term. Since the diffusion of submarine pipeline leakage varies with time, a standard  $k$ - $\epsilon$  model is selected as the turbulence model with the adoption of unsteady simulation. In addition, the gravity factor is considered in the operating environment. The realizable  $k$ - $\epsilon$  turbulence model includes two equations of turbulent kinetic energy and turbulent energy dissipation rate.

$$\rho \frac{\partial \epsilon}{\partial t} + \rho u_i \frac{\partial \epsilon}{\partial x_i} = \frac{\partial}{\partial x_j} \left[ \left( \mu + \frac{\mu_t}{\sigma_\epsilon} \right) \frac{\partial \epsilon}{\partial x_j} \right] + \rho C_1 S \epsilon - \rho \quad (8)$$

$$\rho \frac{\partial k}{\partial t} + \rho u_i \frac{\partial k}{\partial x_i} = \frac{\partial}{\partial x_i} \left[ \left( \mu + \frac{\mu_t}{\sigma_k} \right) \frac{\partial k}{\partial x_j} \right] + G_k + G_b - \rho \epsilon \quad (9)$$

$$G_k = -\rho \overline{u_i' u_j'} \frac{\partial u_j}{\partial x_j} \quad (10)$$

$$G_b = -g \frac{\mu_t}{Pr_t} \frac{\partial \rho}{\partial x_i} \quad (11)$$

in which  $G_k$  stands for the kinetic energy that is turbulent due to the mean velocity gradient,  $\mu$  and  $\mu_t$  are the dynamic viscosity and turbulent viscosity of the fluid, respectively,  $k$  and  $\epsilon$

are the production and dissipation rate of turbulence kinetic energy, respectively,  $\sigma_k$  and  $\sigma_\epsilon$  are the dynamic viscosity and turbulent viscosity of the fluid, respectively.

$$\mu_t = \rho C_\mu \frac{k^2}{\epsilon} \quad (12)$$

where  $S$  is the modulus of the mean rate of strain tensor as follows:

$$S = \sqrt{2S_{ij} \cdot S_{ij}} \quad (13)$$

$$S_{ij} = \frac{1}{2} \left( \frac{\partial u_i}{\partial x_j} + \frac{\partial u_j}{\partial x_i} \right) \quad (14)$$

The coefficients appearing in the model are known as  $C_1 = \max\left(0.43, \frac{\eta}{\eta+5}\right)$ ,  $\eta = S \frac{k}{\epsilon}$ ,  $C_1 = 1.44$ ,  $C_2 = 1.92$ ,  $C_\epsilon = 1$ ,  $C_\mu = 0.09$ ,  $Pr_t = 0.85$ ,  $\sigma_k = 1$ ,  $\sigma_\epsilon = 1.2$ .

### 3. Numerical Model Verification

#### 3.1. Experiment Settings

In order to study the water and gas two-phase distribution rule after porous leakage and diffusion of submarine pipelines, the real condition of submarine gas pipelines is simulated using the sealed steel pipes with nitrogen injected. By immediately opening the leak valves on the steel pipes, undersea pipeline leakages are simulated.

The integrated design of the experimental apparatus employed in this study is depicted in Figure 1, which primarily comprises a nitrogen delivery system (nitrogen bottle with pressure reducing valve to control and keep the gas pressure unchanged), an experimental water tank, a sealed steel pipe fitted with a leak valve, a high-speed camera system, and a signal acquisition system. In the sealed steel pipe, the nitrogen pressure can be maintained consistently by the nitrogen delivery system. The depth of the test water tank is 0.4 m. The leak valve is installed using a sealed steel pipe that is 1 m long and 0.06 m in diameter. When the leaky valve is opened, three leaks have a diameter of 0.006 m and a height of 0.1 m below the water's surface. The undersea leakage process can be entirely recorded and saved using the high-speed camera system and signal acquisition system.

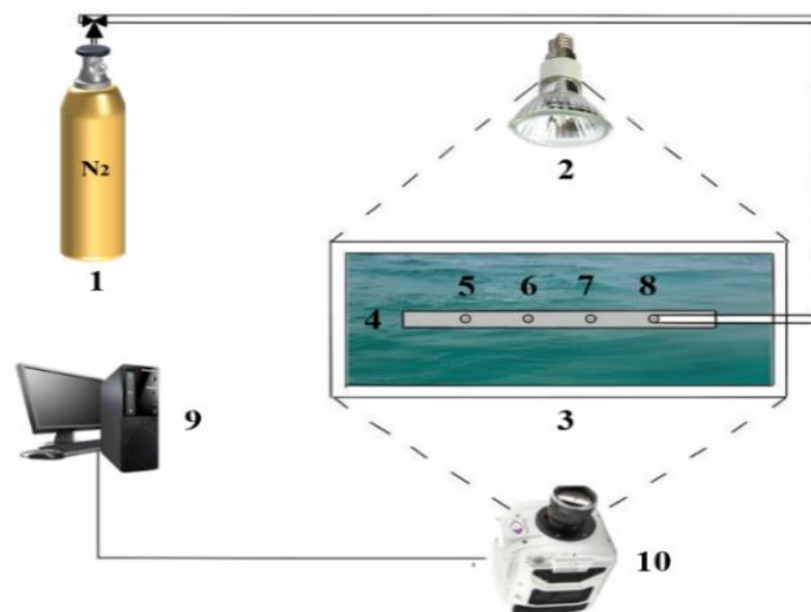


**Figure 1.** Experimental platform: (1) N<sub>2</sub>; (2) light-source; (3) water tank; (4) sealed steel pipe; (5) leakage valve 1; (6) leakage valve 2; (7) leakage valve 3; (8) nitrogen delivery system; (9) signal acquisition system; (10) high-speed camera system.

### 3.2. Comparative Analysis of Experimental and Simulation Results

A model size in the experiment is selected for simulation. The size of the 2D grid model is set as  $0.6\text{ m} \times 2\text{ m}$ . There are three leakage pores with leakage pore size of  $0.006\text{ m}$ . Grid meshing is done using a structured grid, and while the leaky pore is operating at  $91.23\text{ m/s}$ . The calculation area and boundary condition settings are shown in Figure 2.

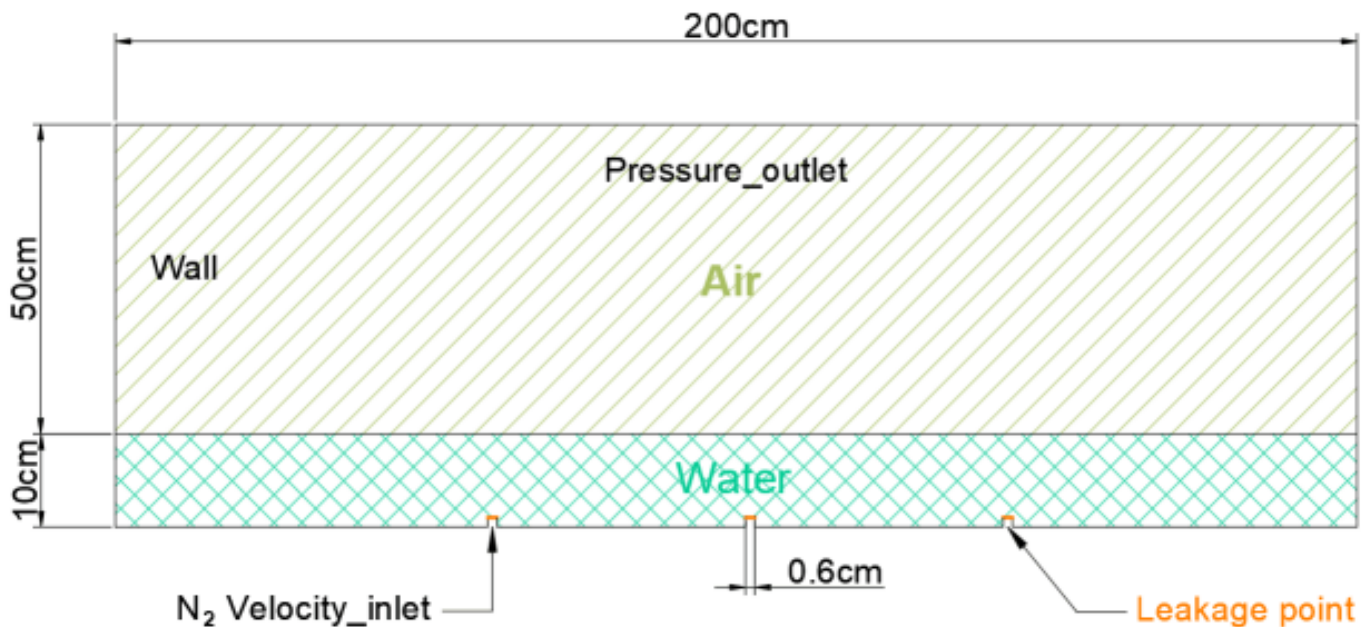


Figure 2. Leakage experiment diagram.

The valve's opening is utilized to mimic the creation of a leaky hole. The time is  $t = 0\text{ s}$  when the first valve is opened,  $t = 1\text{ s}$  when the second valve is opened, and  $t = 2\text{ s}$  when the third valve is opened.

It can be shown, by comparing and evaluating the times  $t = 0.004\text{ s}$ ,  $t = 1.004\text{ s}$ , and  $t = 2.004\text{ s}$ , that at the start of the leakage, the air mass is rising due to the jet's kinetic energy and the buoyancy of the water at the leakage port. As the bubble moves further from the leak, water significantly resists the air mass, which causes the rising speed to slow down without the addition of leakage energy. Through a comparison of the data for  $t = 0.160\text{ s}$ ,  $t = 1.160\text{ s}$ , and  $t = 2.160\text{ s}$ , it can be seen that the air mass gradually assumes a mushroom shape as the additional growing speed of the leakage energy near the leakage port increases. When  $t = 0.120\text{ s}$ ,  $t = 1.120\text{ s}$ , and  $t = 2.120\text{ s}$  are compared and analyzed, it becomes clear that during the rising process, the atmosphere is continuously split up into small bubbles, the degree of mixing with water grows, and the range of bubbles formed expands. It is clear from comparing and studying  $t = 0.080\text{ s}$ ,  $t = 1.080\text{ s}$ , and  $t = 2.080\text{ s}$  that the range of the bubble plume will keep expanding as the air mass rises, as shown in Figure 3.

Water and gas two-phase distribution at stable leakage is acquired by a high-speed camera on the experimental platform of porous leakage in underwater pipelines, which is then processed and analyzed. Three subplots of the experiment's water-gas distribution (left in Figure 4) are compared with those at the corresponding simulation moments. Both flow states are consistent after analysis, demonstrating the accuracy and dependability of the porous leakage model designed for undersea pipes.

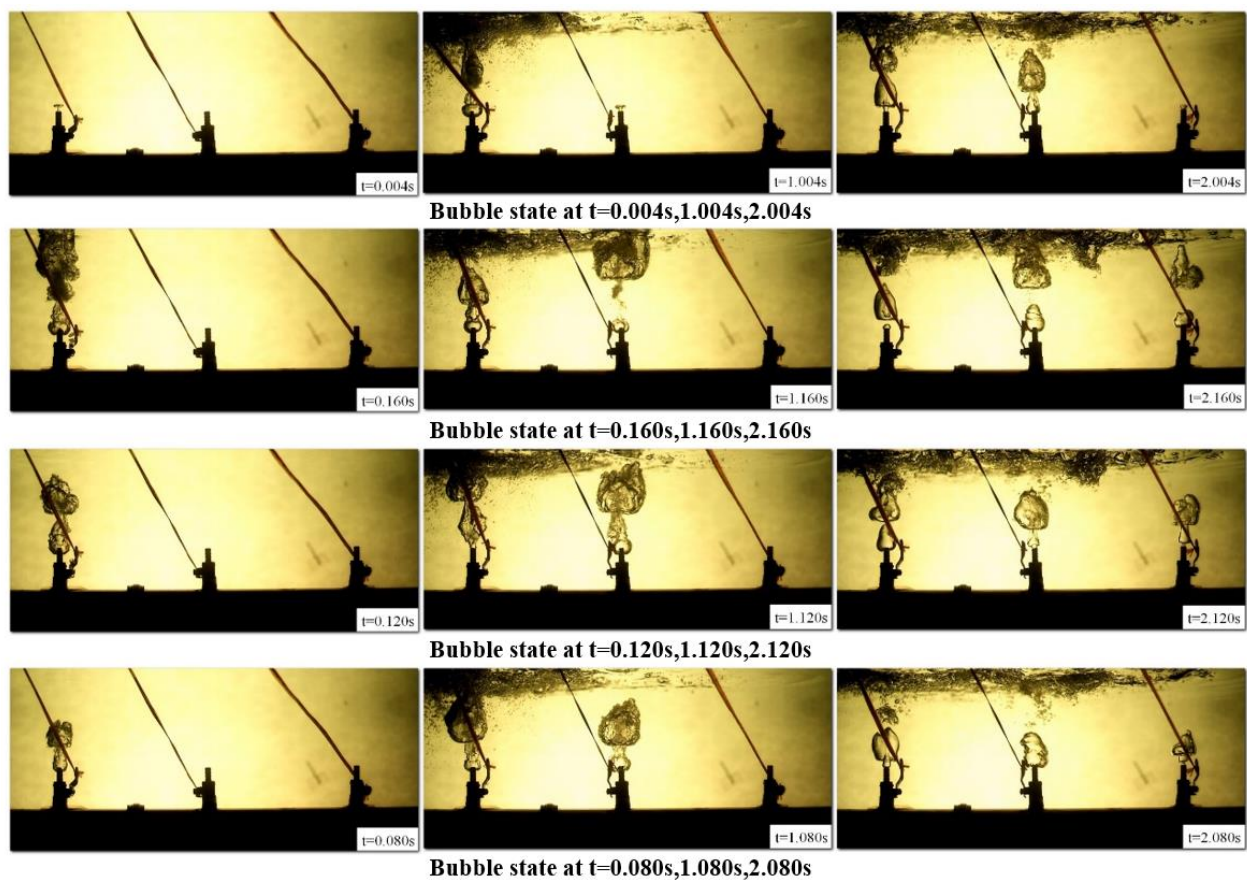


Figure 3. Bubble state in different periods.

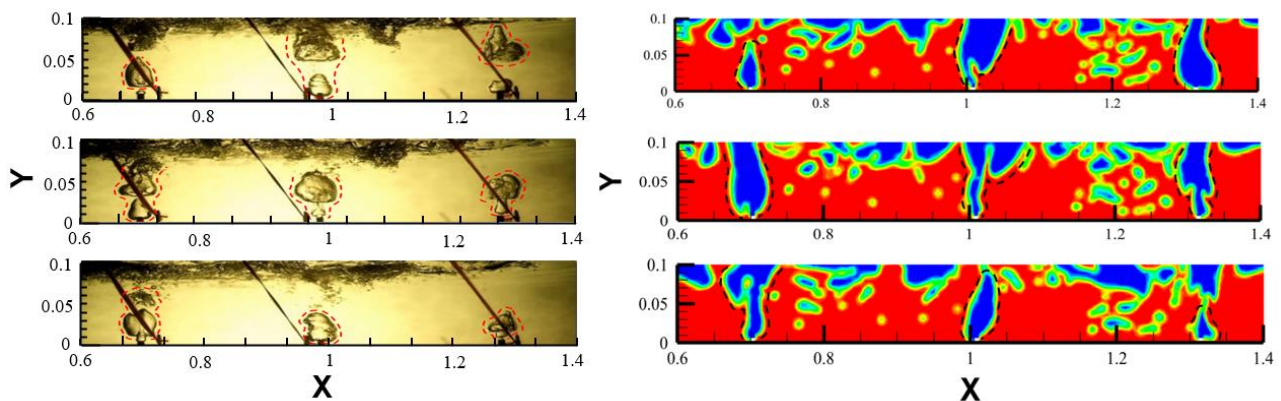


Figure 4. Water and gas two-phase distribution at stable leakage.

## 4. Results and Discussion

### 4.1. Orthogonal Test Simulation Using Mathematics

Only a certain factor affecting the diffusion of porous leakage for submarine gas-delivering pipelines can be determined through the single-factor experiment under unchanged conditions. In that case, the master-subordinate relationship between each factor cannot be determined. Thus, in order to study the master-subordinate relationship of the influence of the leakage velocity, the size of leakage pore, and the velocity of ocean current on the porous leakage of submarine gas-delivering pipelines, the experiment is designed with the orthogonal test method. Additionally, thorough comparison and range analysis are used to evaluate the experimental data in order to identify the master-subordinate relationships among the variables influencing how quickly gas diffuses to the sea surface.

Based on the EGIG statistics of the probability of occurrence of small-pore leakage, perforating leakage, and pipeline rupture in the submarine pipeline, the sum of the probabilities of small-pore leakage and perforating leakage is about 83% in the case of leakage in the gas-delivering pipeline. Consequently, the equivalent diameters of 20 mm, 50 mm, and 100 mm are taken as representative sizes to conduct detailed studies on the natural gas leakage of perforating submarine pipelines and ruptured submarine pipelines. Multiple pores typically leak simultaneously in the submarine pipelines. When three pores simultaneously leak, three leakage pores are configured to examine the entire leakage process in undersea pipelines. Vortex and other influencing elements will be produced as a result of the interaction between gas and liquid, and they will have an impact on the leakage range of the pipelines. The delivery pressure and delivery temperature of submarine pipelines are set as 5 MPa (absolute pressure) and 27 °C, respectively. The leakage velocity of natural gas is calculated as 240 m/s. On the premise that the velocity of natural gas leakage is fixed, the leakage velocity of the reference groups is set at 180 m/s and 300 m/s to analyze the influence of leakage velocity on the leakage process of submarine pipelines.

The ocean current velocity is set for simulation testing at 0.2, 0.35, and 0.5 m/s to study the effect of ocean current movement on the diffusion rule of gas leaks for underwater pipes.

The final factors selected and their levels are shown in Table 1:

**Table 1.** Levels of diffusion factors for leaking submarine pipelines.

Item	Level		
	1	2	3
A: Leak rate/(m·s <sup>-1</sup> )	180	240	300
B: Leak diameter/(m)	0.02	0.05	0.10
C: Water velocity/(m·s <sup>-1</sup> )	0.20	0.35	0.50

For the control variable approach to be used to choose a single factor for one-by-one analysis, 3<sup>3</sup> tests are necessary to handle the issues of three factors and three levels. In contrast, the orthogonal test method saves two thirds of the simulation time by requiring only nine simulation tests to produce reliable and scientific results.

An L<sub>9</sub>(3<sup>4</sup>) orthogonal array is selected to arrange tests based on the test scheme shown in Table 2.

**Table 2.** Orthogonal test scheme design.

Case	Item		
	A	B	C
1	180	0.02	0.20
2	180	0.05	0.35
3	180	0.10	0.50
4	240	0.02	0.35
5	240	0.05	0.50
6	240	0.10	0.20
7	300	0.02	0.50
8	300	0.05	0.20
9	300	0.10	0.35

According to the leakage diffusion model designed by the orthogonal test method, the size of the 2D grid model is 40 m × 90 m. The step length is 0.005 s, the total time step is 5.53 × 10<sup>2</sup>, and the total time is 2.765 s. The maximum mesh size is 0.2 m, and a structured grid is adopted for grid partitioning, with the number of grids being 45,533. Meanwhile, the vicinity of the leakage pores should be encrypted in operation. Calculation area and boundary condition settings are shown in Figure 5. The grid is partitioned and the grid near the three leakage points is refined, as shown in Figure 6.

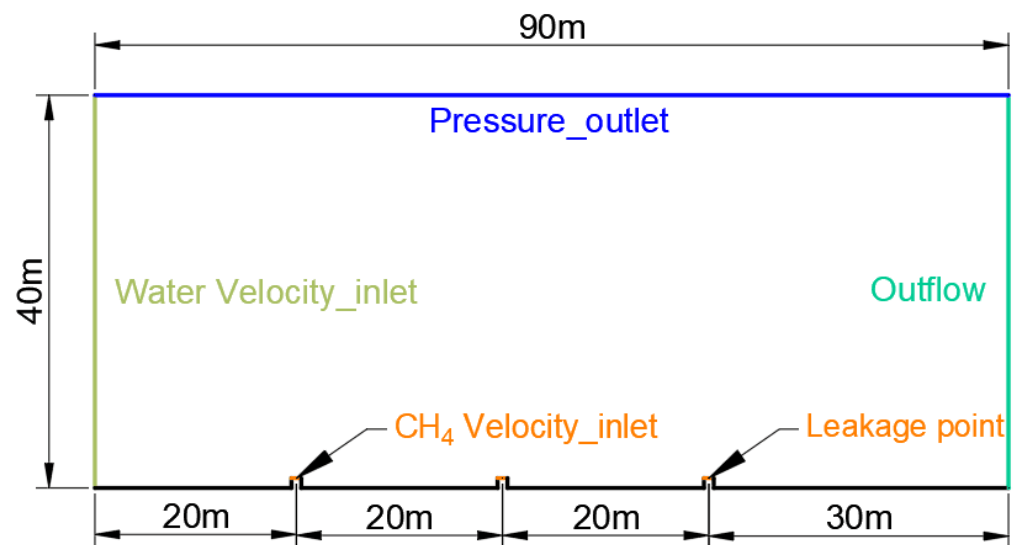


Figure 5. The leakage model.

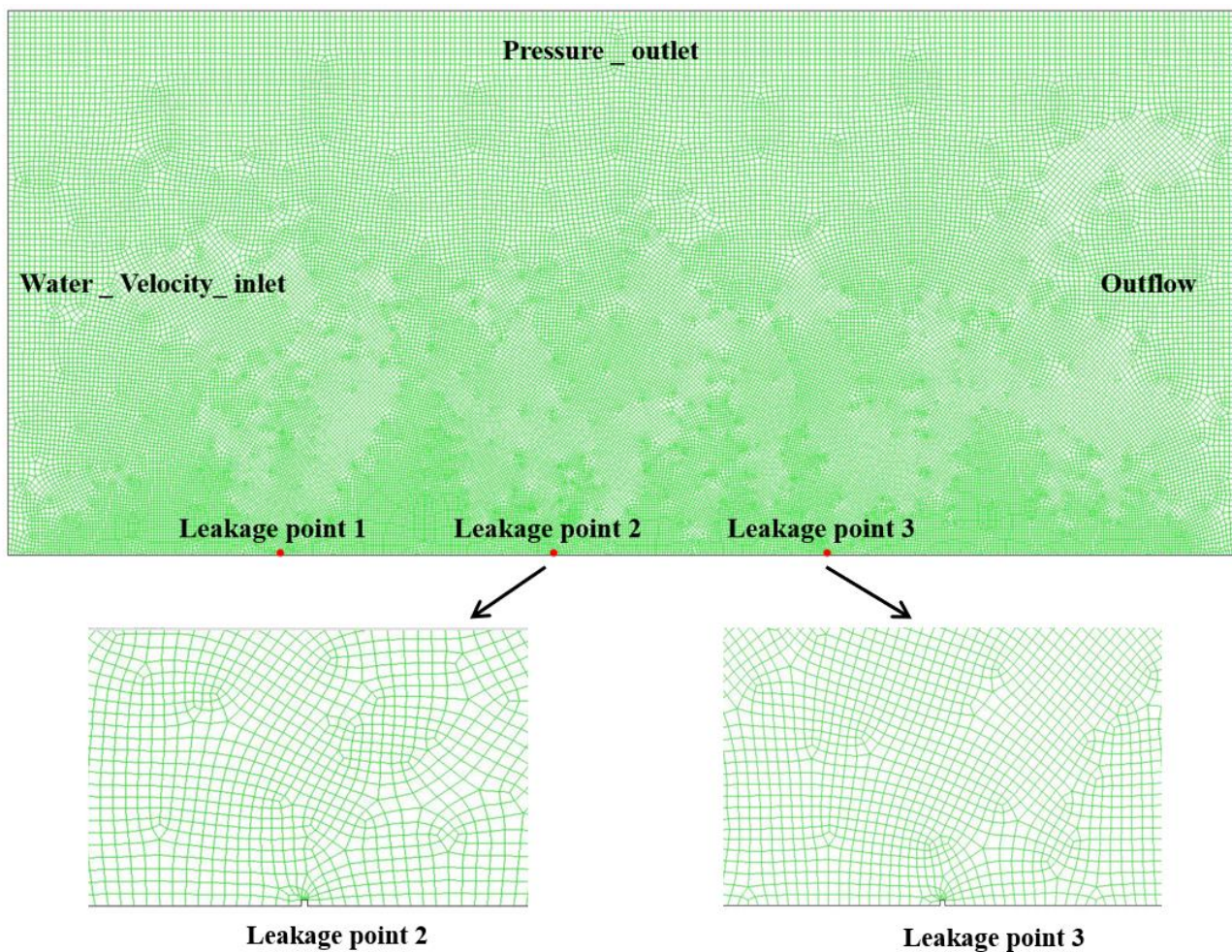
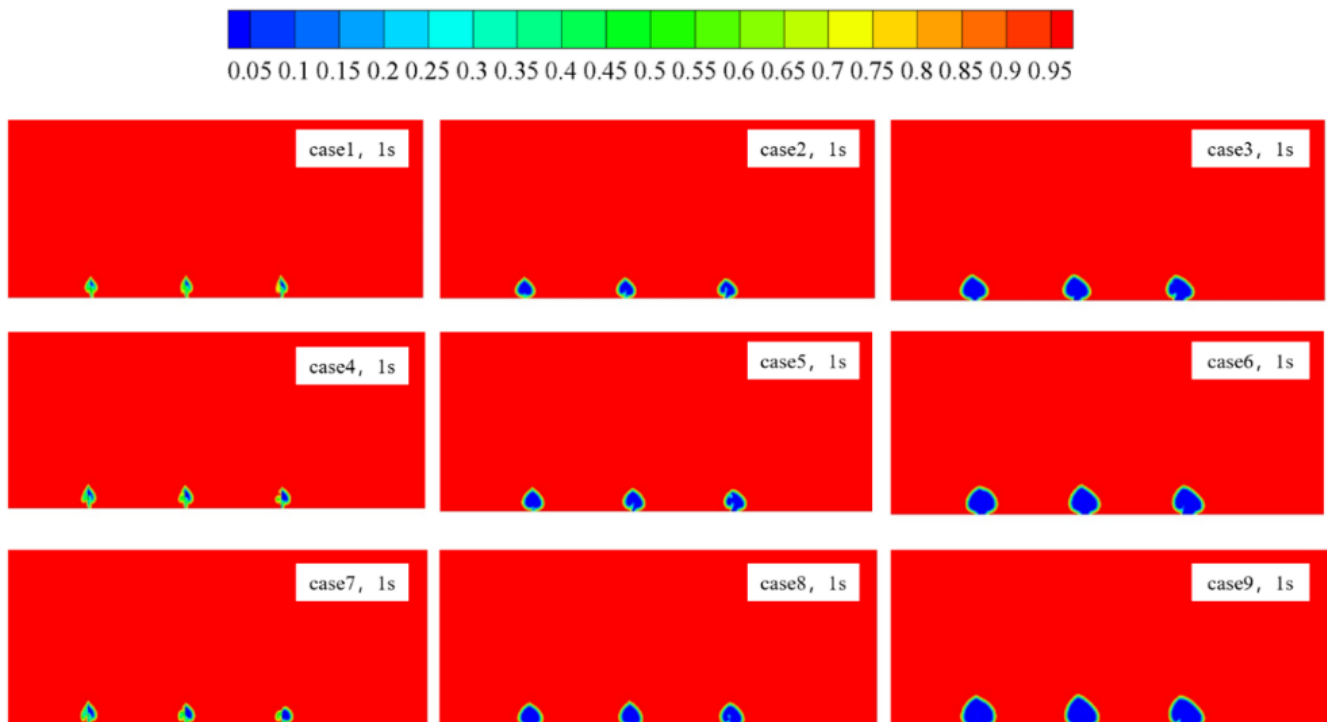


Figure 6. Model meshing.

With regard to how undersea pipeline leakage and diffusion are calculated, the following assumptions are made: 1. With a constant leakage velocity, the leakage pore's pressure is expected to remain constant throughout the whole leakage process; 2. Methane is the sole component of natural gas; 3. Seawater and methane gas energy transfer is disregarded.

#### 4.2. Factors Influencing Underwater Gas Diffusion

In the early stage of leakage, air mass is raised continuously under the effect of the kinetic energy during ejection from the leakage outlet. When the air mass is strongly resisted by water without an energy boost from the leakage outlet, the velocity of the air mass slows down at the location far from the leaking pore. Additionally, the leaking port's consistent energy gain causes the mushroom-shaped air mass nearby to move faster. Bubble diagrams formed above the leaked positions after gas leakage for 1 s of each test scheme are shown in Figure 7.



**Figure 7.** Gas distribution after gas leakage for 1 s.

By comparing Figure 7 (case 1, case 2, case 3), Figure 7 (case 4, case 5, case 6) and Figure 7 (case 7, case 8, case 9), it can be observed that the size of the air mass is closely related to the size of the leakage pore, that is, the larger the leakage pore, the larger the radius of air mass formed. By comparing Figure 7 (case 1, case 4, case 7), Figure 7 (case 2, case 5, case 8), and Figure 7 (case 3, case 6, case 9), it can be observed that the size of the air mass is also related to the leakage velocity, that is, the greater the leakage velocity, the larger the size of air mass. It shall be noted that the correlated influence of leakage velocity is greater than that of the leakage radius. By comparing Figure 7 (case 1, case 5, case 9), Figure 7 (case 2, case 6, case 7), and Figure 7 (case 3, case 4, case 8), it can be observed that the initial shape and size of the air mass have no obvious relation with the velocity of the ocean current.

Under the combined influence of buoyancy force, inertial force, and ocean current force, the created air mass is broken up into bubbles and propelled higher. At the same time, the bubble plume range is also expanded. As a huge air mass is broken up into little bubbles, the degree of bubble mixing with seawater increases. The amount of gas leaking per unit of time results in various shapes of air mass in saltwater depending on the size of the leakage pore and the leakage velocity. The diffusion of gas leakage of each simulation test after leaking for 5 s is shown in Figure 8.

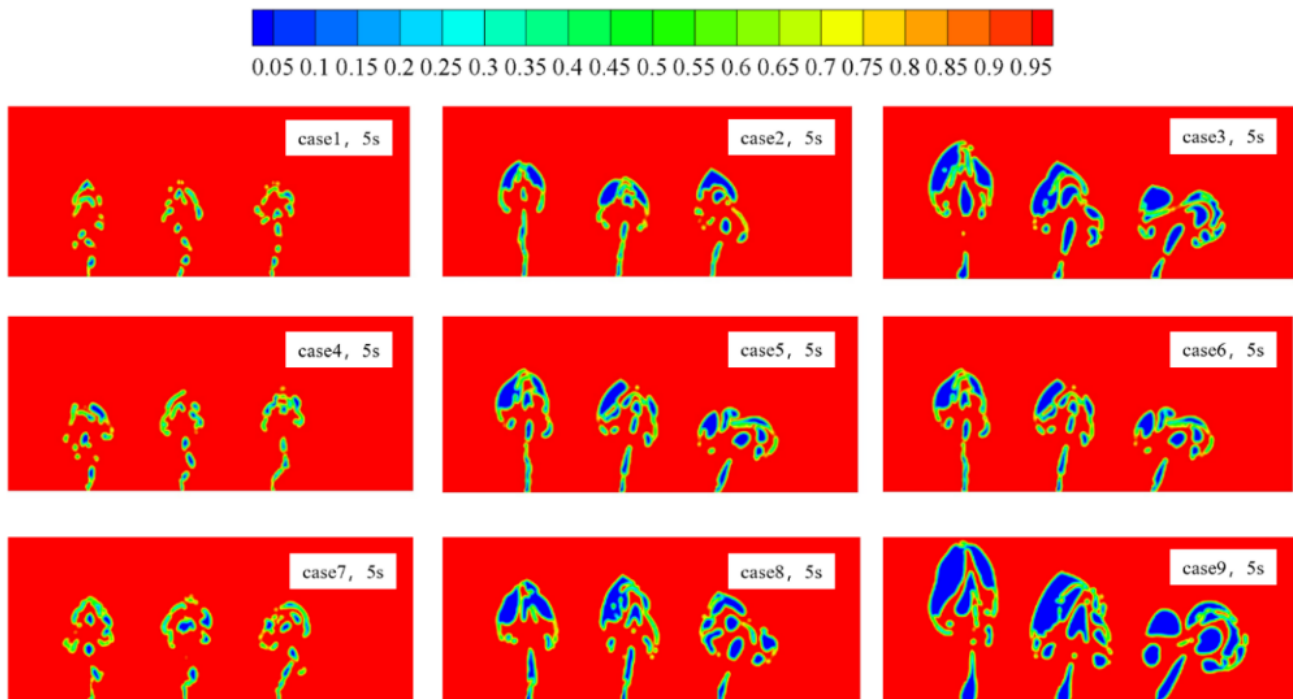


**Figure 8.** Gas distribution after gas leakage for 5 s.

By comparing Figure 8 (case 1, case 2, case 3), Figure 8 (case 4, case 5, case 6), and Figure 8 (case 7, case 8, case 9), it can be observed that the mixing diffusion of gas and seawater is significantly affected by the size of leakage pore; the larger the size of leakage pore in diameter, the smaller the mixing degree of gas and seawater and the larger the bubble radius. By comparing Figure 8 (case 1, case 4, case 7), Figure 8 (case 2, case 5, case 8), and Figure 8 (case 3, case 6, case 9), it can be observed that the mixing degree of gas and seawater is also highly correlated with the leakage velocity. The leakage capacity increases with the reduced mixing degree of gas and seawater and the increase of bubble radius. However, the influence of the velocity of leakage diffusion is far lower than that of the size of leakage pore. The gas leakage is greatly influenced by the ocean current when the leakage velocity is lower, and the bubbles at the leakage port will travel somewhat in the direction of the water flow. There will be a modest influence of ocean current on the gas leakage when the leakage velocity is high and the leakage amount is considerable. By comparing Figure 8 (case 1, case 5, case 9), Figure 8 (case 2, case 6, case 7), and Figure 8 (case 3, case 4, case 8), it can be observed that the shape of gas leakage and diffusion in seawater is significantly affected by the velocity of the ocean current; the speed of the ocean current directly influences the horizontal component velocity of water bubbles. Therefore, the greater the current velocity, the greater the bubble's horizontal velocity, the farther the bubble moves horizontally in one direction per unit of time, and the broader the diffusion range and the various diffusion modes.

The time and shape of gas may vary when the leakage gas floats to the sea surface as these are affected by the leakage velocity, the leakage pore size, and the velocity of ocean current. The gas distribution when the leaked gas reaches the sea surface and the time required for the leaked gas to reach the sea surface are shown in Figure 9.

By comparing Figure 9 (case 1, case 2, case 3), Figure 9 (case 4, case 5, case 6), and Figure 9 (case 7, case 8, case 9), it can be observed that the time when the gas reaches the sea surface and the shape of the bubble during leakage are significantly affected by the size of leakage pore. The ocean current's influence on the water bubble will be minimal when the leakage pore size is big. In that case, there will be also a low degree of mixing with sea water with a reduced time for reaching the sea surface. By comparing Figure 9 (case 1, case 4, case 7), Figure 9 (case 2, case 5, case 8), and Figure 9 (case 3, case 6, case 9), it can be

observed that the greater the leakage velocity, the smaller the mixing degree of the leaked gas and seawater. The time it takes for the leaking gas to reach the sea surface will decrease as the diffused bubble's volume rises. Under the assumption that seawater depth remains constant, the vertical velocity of the air mass will increase when the leakage velocity is high; this will reduce the time it takes the gas to reach the sea surface. In addition, the unchanged horizontal component velocity will result in a decreased horizontal gas migration distance. By comparing Figure 9 (case 1, case 5, case 9), Figure 9 (case 2, case 6, case 7), and Figure 9 (case 3, case 4, case 8), it can be observed that gas leakage is significantly affected by the velocity of the ocean current when it is diffused to the sea surface. The distance of the horizontal movement of the bubble in the water increases together with the distance of the leak hole in the direction of the ocean current and the influence of the current velocity. The vertical velocity of the bubble will diminish as it reaches a particular height. The component velocity in the horizontal direction, which depends on the ocean current velocity, has a significant impact on the bubble's final velocity. At this point, the range of gas diffusing to the sea surface increases with increasing ocean current velocity.

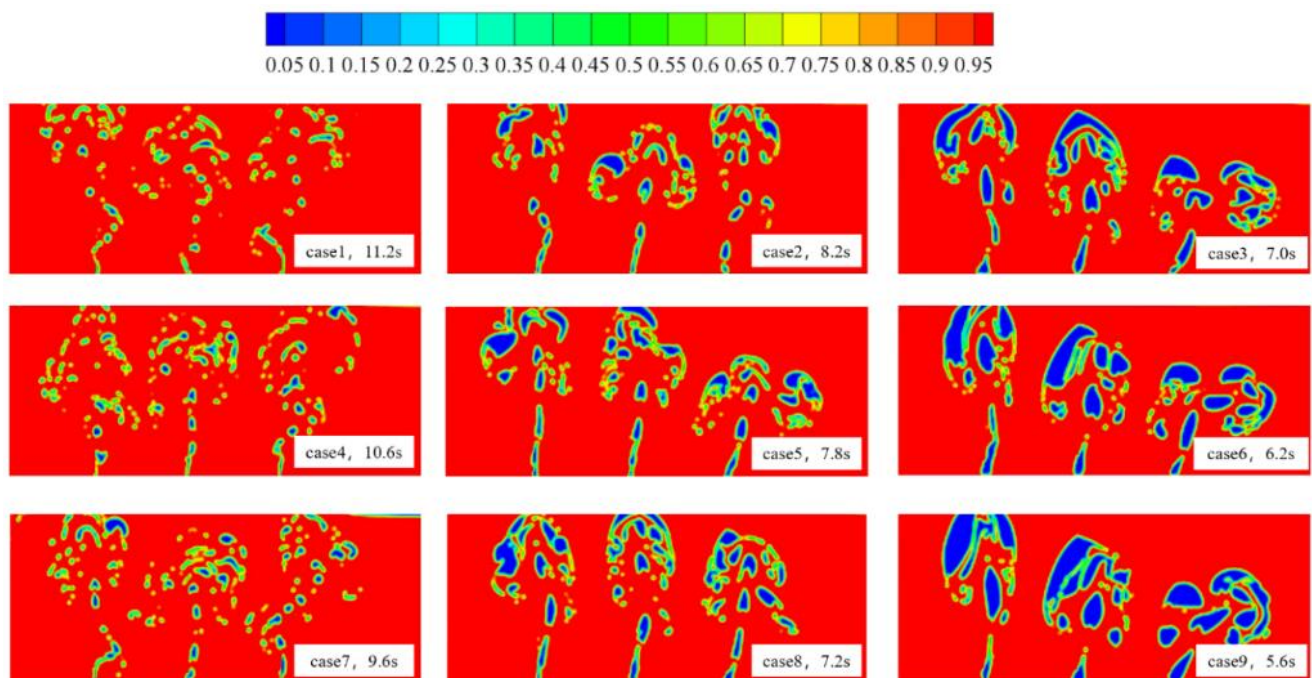


**Figure 9.** Gas distribution at the moment of leaked gas reaching the sea surface.

#### 4.3. Analysis of Porous Effect

The influence of three leakage pores can be analyzed by taking the example of the leaked natural gas reaching the water surface at 5.6 s in experiment 9. According to the Figure 10, the influence of leakage pores effects the diffusion in the horizontal direction. Thus, it can start from analyzing the vector field along the x direction, as shown in Figure 10. The natural gas moves upwards quickly when reaching the sea water, causing both sides of seawater to be moved downwards to generate a strong back flow. As the passage of time passes, a powerful turbulent motion develops between the two fluids as the gas continues to rise upward alongside the seawater's backflow. This turbulent motion will shift rightwards at the horizontal velocity to increase the horizontal component velocity of sea water.

The final distribution of velocity directions is shown in Figure 10, and the velocity isoline distribution is shown in Figure 11. It is obvious that the speed at which the turbulent motion forms can be as high as 14 m/s along the positive direction of x and 8 m/s along the negative direction of x, which is significantly faster than the ocean current's speed of 0.35 m/s. As a result of the turbulent interaction between several pores, the strong

turbulent motion at leakage hole 1 causes the horizontal component velocity of seawater to increase to the right, and the velocity on the right side of leaking hole 3 increases due to the superposition of turbulent motion at locations 1 and 2. Therefore, the diffusion range of natural gas is increased. The analysis above demonstrates that when porous leakage occurs in submarine pipelines, multiple leaking pores are mutually affected. The “butterfly effect” will occur between leakage pores as a result of turbulent motion and ocean current; the closer the leakage hole is downstream along the direction of the ocean current, the wider the range of the natural gas leakage reaching the sea surface.

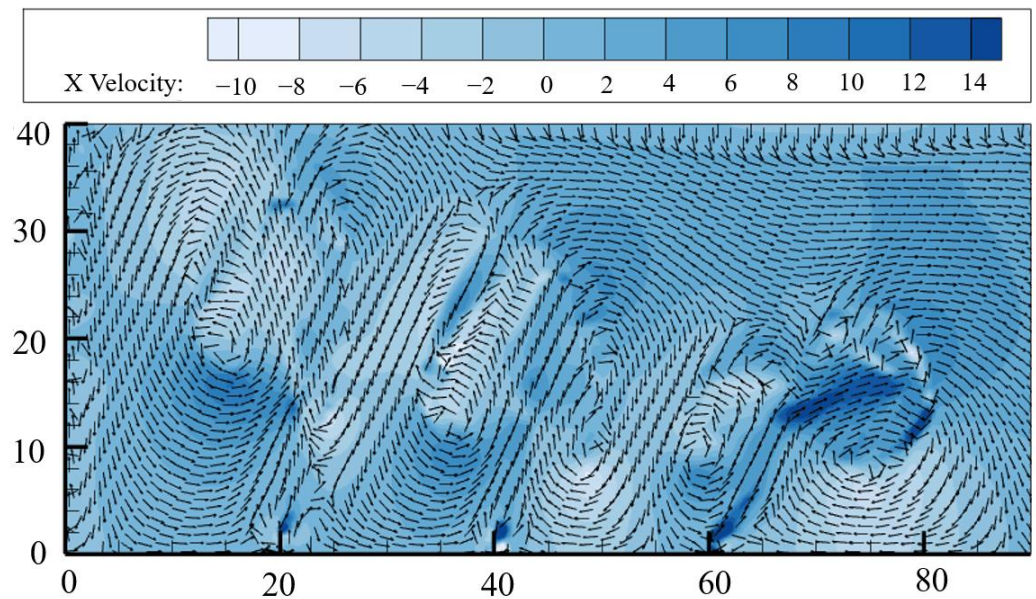


Figure 10. Velocity vector of test 9 at 5.6 s.

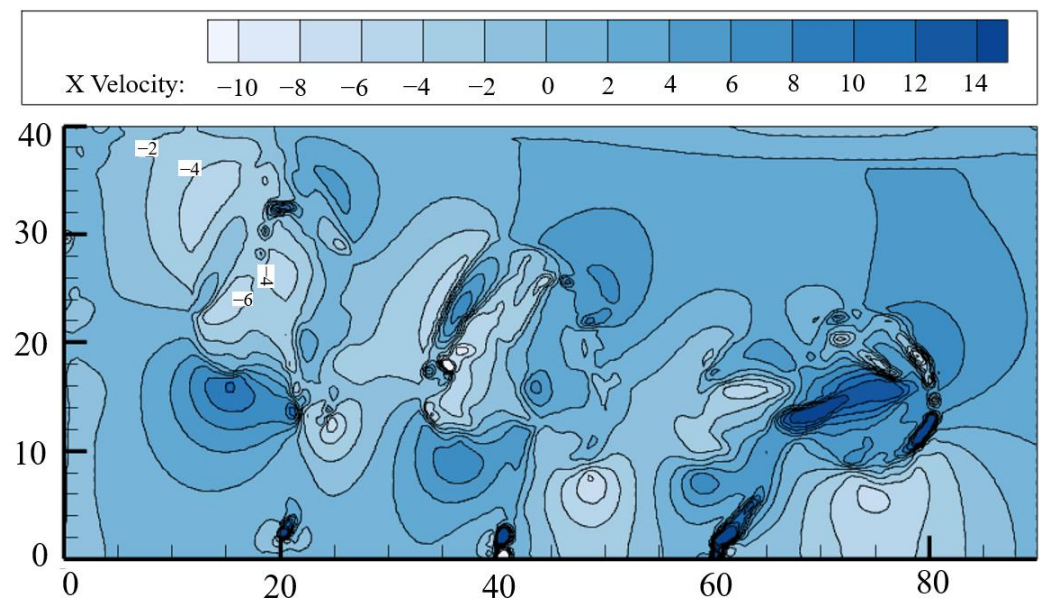


Figure 11. Velocity isoline of test 9 at 5.6 s.

#### 4.4. Multi-Factor Coupling Analysis

The master–subordinate relationship and the relevance of each affecting element on test indexes cannot be determined quantitatively, despite the comprehensive comparison’s ability to show the influence of each affecting item on the leaked findings. In order to determine the master–subordinate relationship and significance of each affecting factor, specific indexes should be compared and analyzed.

By using range analysis and using the results of numerical simulation as the index, it is possible to determine the master–subordinate relationship between the factors affecting how long it takes for the bubble to reach the sea surface. The design of the test scheme and analysis of the results are shown in Table 3, where  $k_i$  is the average of indicators corresponding to the  $i$  level of each factor, and  $R$  is the range of each factor.

**Table 3.** Design of test scheme and displayed result.

Case	Item			Time/s
	A: Leak Rate	B: Leak Diameter	C: Water Velocity	
1	1	1	1	11.2
2	1	2	2	8.2
3	1	3	3	7.0
4	2	1	2	10.6
5	2	2	3	7.8
6	2	3	1	6.2
7	3	1	3	9.6
8	3	2	1	7.2
9	3	3	2	5.6
$k_1$	8.80	10.47	8.20	
$k_2$	8.20	7.73	8.13	
$k_3$	7.47	6.27	8.13	
$R$	1.33	4.20	0.07	

According to the analysis of results shown in Table 3, the ranges of leakage velocity, leakage pore size, and the velocity of ocean current are 1.33, 4.2, and 0.07, respectively. The greater the range, the greater the influence of the corresponding factor on the indicator; specifically, the more important the factor will be.  $R_2 > R_1 > R_3$  indicates the master–subordinate relationship of leakage velocity, the size of the leakage pore, and the velocity of the ocean current, as shown below:

Size of leakage pore > Leakage velocity > Velocity of ocean current.

With the factor level as the x-coordinate and the average of the index as the y-coordinate, factors and index trends are produced in order to intuitively depict the influence rule and trend of factors on indexes. An orthogonal experiment can be used to quantify the influence of several factors; the greater the slope of the influencing factors, the greater the influence, as illustrated in Figure 12.

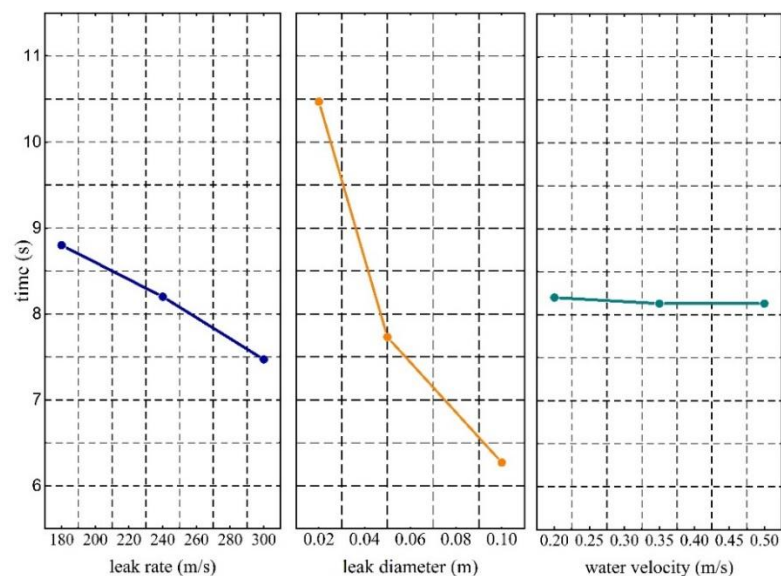


**Figure 12.** Trend of factor index.

It can be seen in the figure that the influence of the size of the leakage pore on the time of reaching the sea surface is much higher than that of the water velocity, as the influence of water velocity is so small that it can be ignored.

## 5. Principle of Similitude

### 5.1. Similitude Theory

Similarity theory is a theory that explains the similarity principle of all similar phenomena in nature and engineering. It is a theory that examines how individuality and generalization (or the particular and the general) and internal and outward conflicts in natural events interact. It is mostly used to direct model testing and assess how closely the “model” and “prototype” compare.

### 5.2. Similitude Experimental Design

Liquid motion occurs in a specific space and time and abides by the fundamental principles of fluid kinematics and dynamics. The three types of physical quantities used to depict fluid motion processes are flow field geometry, motion state, and dynamic properties. When the single-valued conditions (such as the system’s geometric properties, the medium’s physical properties, the initial conditions, and the boundary conditions, etc.) are similar to one another, and the similarity criteria made up of the physical quantities of the single-valued conditions have numerical values that are equal, all phenomena with the same property must be similar. Geometric, dynamic, and kinematic similarity between two related flow systems must be ensured.

In order for two flows to be geometrically comparable, their corresponding line segments must be proportional, their angles must be equal, and their boundary characteristics (such as the roughness of the solid boundary or the free liquid surface) must be the same. To be more specific, if N geometry is length  $l$ , area  $A$ , and volume  $V$ , then the similarity constants are expressed as follows ( $p$  and  $m$  represent prototype and model respectively):

$$\lambda_l = \frac{l_p}{l_m} \quad (15)$$

$$\lambda_A = \frac{A_p}{A_m} = \lambda_l^2 \quad (16)$$

$$\lambda_V = \frac{V_p}{V_m} = \lambda_l^3 \quad (17)$$

Among the subsea pipelines laid, small diameter pipelines range from 50.8 to 254 mm (2 to 10 in), medium diameter pipelines range from 304.8 to 609 mm (12 to 24 in), and large diameter pipelines range from 609.6 to 863.6 mm (24 to 34 in). Taking Bohai Sea as an example, the inner diameter of the submarine oil pipeline is 219 mm. According to the actual situation, the similarity ratio between the model and the prototype pipe diameter is 1:3.65.

$$\lambda_l = \frac{l_p}{l_m} = 3.65 \quad (18)$$

$$\lambda_A = \frac{A_p}{A_m} = \lambda_l^2 = 3.65^2 \quad (19)$$

$$\lambda_V = \frac{V_p}{V_m} = \lambda_l^3 = 3.65^3 \quad (20)$$

At the corresponding places of two flows, dynamic similarity refers to the proportionate dynamic quantities of the same name. It mainly refers to the force acting on the fluid, including gravity  $G$ , viscous force  $T$ , pressure  $P$ , elastic force  $E$ , etc. Gravity plays a leading role in the process of underwater gas leakage. The Froude number of the prototype and model is the same when using the gravity similarity criterion.

Then

$$F_{r_p} = F_{r_m} \quad (21)$$

$$\frac{v_p^2}{g_p l_p} = \frac{v_m^2}{g_m l_m} \quad (22)$$

The similar constant of density

$$\lambda_\rho = \frac{\rho_p}{\rho_m} = 1 \quad (23)$$

The similar constant of gravity acceleration

$$\lambda_g = \frac{g_p}{g_m} = 1 \quad (24)$$

The similar constant of quality

$$\lambda_m = \frac{m_p}{m_m} = \frac{\rho_p V_p}{\rho_m V_m} = \lambda_\rho \lambda_V = \lambda_l^3 = 3.65^3 \quad (25)$$

The similar constant of gravity

$$\lambda_G = \lambda_m \lambda_g = \lambda_l^3 = 3.65^3 \quad (26)$$

Kinematic similarity refers to the kinematic range ratio of the same name at the corresponding points of two flows. The trajectories of analogous fluid particles in two flows with similar motion should also be geometrically similar, and the amount of time that they spend flowing through corresponding line segments on corresponding trajectory lines should likewise be proportional. Assuming that  $v_p$  is the flow rate at a certain point in the prototype machine and  $v_m$  is the flow rate at the corresponding point in the model, then the scale of the flow rate is:

$$\lambda_v = \frac{v_p}{v_m} \quad (27)$$

According to the Froude similarity criterion, the following can be obtained:

$$\lambda_v = \frac{v_p}{v_m} = \left( \frac{l_p}{l_m} \right)^{\frac{1}{2}} = \sqrt{3.65} \quad (28)$$

$$\lambda_t = \frac{t_p}{t_m} = \frac{\lambda_l}{\lambda_v} = \sqrt{3.65} \quad (29)$$

## 6. Conclusions

Using the Volume of Fluid (VOF) approach and computational fluid dynamics (CFD) method, the porosity leaking diffusion process of undersea gas pipelines can be simulated. Experiments are used to confirm that the simulation is accurate and reliable. At the same time, the orthogonal experiment method is used to select the influence of natural gas pipeline leakage pores, leakage velocity, and ocean current velocity on the coupling effect of underwater leakage gas diffusion and the range of porous utility analysis. Additionally, the leakage model is connected to the practical application using the gravity similarity principle.

The size of the leakage hole and the leakage velocity are negatively connected with the time that the leakage gas takes to reach the water's surface, using the time that the leakage gas reaches the sea surface as the indicator. The larger the leakage hole, the larger the leakage capacity, and the shorter the time required for the air mass to reach the water surface. The velocity of the ocean current has little effect on the time for the air mass to reach the water surface but affects the horizontal migration distance of the air mass to the

water surface, that is, the leakage range. The greater the current velocity, the greater the leakage range after reaching the sea surface. As a result, the leaking hole's size has the greatest impact on when the gas leaks into the water, followed by the leakage velocity, with ocean current velocity having the least impact. Through the orthogonal experiment, it is also concluded that the leakage aperture size has the greatest influence on the leakage result, followed by the leakage velocity, and the ocean current velocity leakage has the least influence. When porous leakage occurs in the submarine pipeline, multiple leakage holes affect each other; along the direction of the ocean current velocity, the influence of the leakage hole is more and more obvious, and the range of the leakage gas reaching the sea surface is larger. According to the actual situation, the similarity ratio is determined by using Froude similarity criterion and combining simulation and practice. If we use the big diameter pipeline as an example, the pipe diameter similarity ratio between the model and the prototype is 1:3.65, and the speed and time similarity ratios are both  $1:\sqrt{3.65}$ . The study's findings can offer technical assistance in developing emergency reaction plans for gas leak events in the straits as well as in managing leakage risk and making emergency decisions.

**Author Contributions:** Conceptualization, H.J.; methodology, H.J. and J.G.; software, H.J., H.B. and J.G.; validation, H.J. and J.G.; formal analysis, H.J. and J.G.; investigation, H.J., Y.W. and J.G.; resources, H.J., K.Y., J.J., G.Z. and Z.X.; data curation, H.J., J.G. and Y.W.; writing—original draft, H.J., G.Z. and J.G.; writing—review and editing, H.J.; visualization, H.J. and J.G.; supervision, H.J.; project administration, H.J.; funding acquisition, H.J., K.Y., Z.X. and J.J. All authors have read and agreed to the published version of the manuscript.

**Funding:** This research was funded by the National Natural Science Foundation of China (No.52204204, 51704041, 51574046, 21927815), the Joint Project of Industry-University-Research of Jiangsu Province (No. BY2021421), the Natural Science Foundation of Jiangsu Province (No. BK20150269), and the Major Research Plan of the Oil and Gas Storage and Transportation Laboratory of Jiangsu Province (No. SCZ1211200004/004).

**Data Availability Statement:** The datasets used and/or analyzed during the current study are available from the corresponding author on reasonable request.

**Conflicts of Interest:** The authors declare that they have no known competing financial interests or personal relationships that could have appeared to influence the work reported in this paper.

## References

1. Ji, H.; Xu, M.; Huang, W.; Yang, K. The Influence of Oil leaking rate and Ocean Current Velocity on the Migration and Diffusion of Underwater Oil Spill. *Sci. Rep.* **2020**, *10*, 9226. [[CrossRef](#)] [[PubMed](#)]
2. Mohammadi, L.; Rahdar, A.; Bazrafshan, E.; Dahmardeh, H.; Susan, M.A.B.H.; Kyzas, G.Z. Petroleum Hydrocarbon Removal from Wastewaters: A Review. *Processes* **2020**, *8*, 447. [[CrossRef](#)]
3. Yuan, F.; Zeng, Y.; Luo, R.; Khoo, B.C. Numerical and experimental study on the generation and propagation of negative wave in high-pressure gas pipeline leakage. *J. Loss Prev. Process Ind.* **2020**, *65*, 104129. [[CrossRef](#)]
4. Pan, Y.; Zhai, S.; Meng, X.; Pei, K.; Huo, F. Study on the Fracturing of Rock by High-Speed Water Jet Impact. *Processes* **2022**, *11*, 114. [[CrossRef](#)]
5. Yang, Y.; Khan, F.; Thodi, P.; Abbassi, R. Corrosion induced failure analysis of subsea pipelines. *Reliab. Eng. Syst. Saf.* **2017**, *159*, 214–222. [[CrossRef](#)]
6. Arzaghi, E.; Abbassi, R.; Garaniya, V.; Binns, J.; Chin, C.; Khakzad, N.; Reniers, G. Developing a dynamic model for pitting and corrosion-fatigue damage of subsea pipelines. *Ocean. Eng.* **2018**, *150*, 391–396. [[CrossRef](#)]
7. Li, X.; Chen, G.; Zhu, H. Quantitative risk analysis on leakage failure of submarine oil and gas pipelines using Bayesian network. *Process Saf. Environ. Prot.* **2016**, *103*, 163–173. [[CrossRef](#)]
8. Liang, H.; Li, H.; Hao, X.; Ge, T. Reasons for subsea pipeline failure and ROV-based inspection technology of subsea pipeline. *Oil Gas Storage Transp.* **2015**, *34*, 439–441.
9. Premathilake, L.T.; Yapa, P.D.; Nissanka, I.D.; Kumarage, P. Impact on water surface due to deepwater gas blowouts. *Mar. Pollut. Bull.* **2016**, *112*, 365–374. [[CrossRef](#)]
10. Wang, X.; Luo, J.; Yuan, H.; Luo, Z. Hazard analysis on the offshore natural gas pipelines fatigue failure leakage. *Fire Sci. Technol.* **2018**, *37*, 729–732.
11. Yang, D.; Chen, G.; Shi, J.; Li, X. Effect of gas composition on dispersion characteristics of blowout gas on offshore platform. *Int. J. Nav. Archit. Ocean. Eng.* **2019**, *11*, 914–922. [[CrossRef](#)]

12. Jia, M.; Li, F.; Zhang, Y.; Wu, M.; Li, Y.; Feng, S.; Wang, H.; Chen, H.; Ju, W.; Lin, J.; et al. The Nord Stream pipeline gas leaks released approximately 220,000 tonnes of methane into the atmosphere. *Environ. Sci. Ecotechnol.* **2022**, *12*, 100210. [[CrossRef](#)] [[PubMed](#)]
13. Mocellin, P.; Vianello, C.; Maschio, G. Facing Emerging Risks in Carbon Sequestration Networks. A Comprehensive Source Modelling Approach. *Chem. Eng.* **2018**, *67*, 295–300. [[CrossRef](#)]
14. Hissong, D.W.; Pomeroy, J.; Norris, H.L. A mechanistic model for hydrocarbon plumes rising through water. *J. Loss Prev. Process Ind.* **2014**, *30*, 236–242. [[CrossRef](#)]
15. Hernández-Báez, Á.; Torres, E.S.; Amaya-Gómez, R.; Pradilla, D. Oil Onshore Pipeline Quantitative Risk Assessment under Fire and Explosion Scenarios. *Processes* **2023**, *11*, 557. [[CrossRef](#)]
16. Xinhong, L.; Guoming, C.; Renren, Z.; Hongwei, Z.; Jianmin, F. Simulation and assessment of underwater gas release and dispersion from subsea gas pipelines leak. *Process Saf. Environ. Prot.* **2018**, *119*, 46–57. [[CrossRef](#)]
17. Johansen, Ø. DeepBlow—a Lagrangian Plume Model for Deep Water Blowouts. *Spill Sci. Technol. Bull.* **2000**, *6*, 103–111. [[CrossRef](#)]
18. Bihs, H.; Kamath, A.; Alagan Chella, M.; Arntsen, Ø.A. Breaking-Wave Interaction with Tandem Cylinders under Different Impact Scenarios. *J. Waterw. Port Coast. Ocean. Eng.* **2016**, *142*, 343. [[CrossRef](#)]
19. Cozzuto, G.; Dimakopoulos, A.; De Lataillade, T.; Morillas, P.O.; Kees, C.E. Simulating Oscillatory and Sliding Displacements of Caisson Breakwaters Using a Coupled Approach. *J. Waterw. Port Coast. Ocean. Eng.* **2019**, *145*, 504. [[CrossRef](#)]
20. Li, Q.; Zhou, S.; Wang, Z. Quantitative risk assessment of explosion rescue by integrating CFD modeling with GRNN. *Process Saf. Environ. Prot.* **2021**, *154*, 291–305. [[CrossRef](#)]
21. Paris, C.B.; Henaff, M.L.; Aman, Z.M.; Subramaniam, A.; Helgers, J.; Wang, D.P.; Kourafalou, V.H.; Srinivasan, A. Evolution of the Macondo well blowout: Simulating the effects of the circulation and synthetic dispersants on the subsea oil transport. *Environ. Sci. Technol.* **2012**, *46*, 13293–13302. [[CrossRef](#)] [[PubMed](#)]
22. Zhang, J.; Zheng, J.; Jeng, D.-S.; Guo, Y. Numerical Simulation of Solitary-Wave Propagation over a Steady Current. *J. Waterw. Port Coast. Ocean. Eng.* **2015**, *141*, 281. [[CrossRef](#)]
23. Liu, R.; Ding, S.; Ju, G. Numerical Study of Leakage and Diffusion of Underwater Oil Spill by Using Volume-of-Fluid (VOF) Technique and Remediation Strategies for Clean-Up. *Processes* **2022**, *10*, 2338. [[CrossRef](#)]
24. Cloete, S.; Olsen, J.E.; Skjetne, P. CFD modeling of plume and free surface behavior resulting from a sub-sea gas release. *Appl. Ocean. Res.* **2009**, *31*, 220–225. [[CrossRef](#)]
25. Fan, K.; Wang, W.; Yi, Z.; Liu, R.; Yu, S. Numerical Simulation of Submarine Gas Pipeline Leakage. *Contemp. Chem. Ind.* **2013**, *42*, 503–506.
26. Zhu, P.; Wang, X.S.; Li, G.C.; Liu, Y.P.; Kong, X.X.; Huang, Y.Q.; Yuan, J.W. Experimental study on interaction of water mist spray with high-velocity gas jet. *Fire Saf. J.* **2017**, *93*, 60–73. [[CrossRef](#)]
27. Olsen, J.E.; Skjetne, P. Modelling of underwater bubble plumes and gas dissolution with an Eulerian-Lagrangian CFD model. *Appl. Ocean. Res.* **2016**, *59*, 193–200. [[CrossRef](#)]
28. Zhang, J.; Zang, X.; Zhang, Y.; He, H.; Chen, H. Dynamic characteristics of plume/ jet from underwater pipe downward leakage. *CIESC J.* **2016**, *67*, 4969–4975.
29. Wu, K.; Cunningham, S.; Sivandran, S.; Green, J. Modelling subsea gas releases and resulting gas plumes using Computational Fluid Dynamics. *J. Loss Prev. Process Ind.* **2017**, *49*, 411–417. [[CrossRef](#)]
30. Sun, Y.; Cao, X.; Liang, F.; Bian, J. Investigation on underwater gas leakage and dispersion behaviors based on coupled Eulerian-Lagrangian CFD model-ScienceDirect. *Process Saf. Environ. Prot.* **2020**, *136*, 268–279. [[CrossRef](#)]
31. Zhu, H.; Lin, P.; Pan, Q. A CFD (computational fluid dynamic) simulation for oil leakage from damaged submarine pipeline. *Energy* **2014**, *64*, 887–899. [[CrossRef](#)]
32. Cai, X.; Yu, Y.; Yu, J.; Zhao, S.; Wang, X. Movement Characteristics of Gas Leakage in Shallow Water Pipeline. *China Offshore Platf.* **2018**, *33*, 56–64.
33. Song, J.; Xiao, W.; Li, C.; Chen, H. Simulation and Orthogonal Test Analysis of Leakage Diffusion of Submarine Gas Pipeline. *Oil Field Equip.* **2018**, *47*, 49–56.
34. Ruppel, C.D.; Waite, W.F. Timescales and Processes of Methane Hydrate Formation and Breakdown, With Application to Geologic Systems. *J. Geophys. Res. Solid Earth* **2020**, *125*, e2018JB016459. [[CrossRef](#)]
35. Li, C.; Liu, G. Numerical Simulation for Gas Leakage from Crossing Pipeline under River. *World Sci.-Tech. R D* **2016**, *38*, 564–568.
36. Zhang, Y.; Zhu, J.; Peng, Y.; Pan, J.; Li, Y. Experimental research of flow rate and diffusion behavior of nature gas leakage underwater. *J. Loss Prev. Process Ind.* **2020**, *65*, 104119. [[CrossRef](#)]
37. Ji, H.; Zhang, G.; Yan, K.; Chen, J.; Huang, W.; Huang, F. Numerical Simulation on Single-hole Leakage Shock Wave of Submarine Natural Gas Pipeline. *Saf. Environ. Eng.* **2019**, *26*, 182–186.
38. Mocellin, P.; Vianello, C.; Maschio, G. A comprehensive multiphase CO<sub>2</sub> release model for carbon sequestration QRA purposes. Modeling and conditions for simplifying assumptions and solid CO<sub>2</sub> occurrence. *Process Saf. Environ. Prot.* **2019**, *126*, 167–181. [[CrossRef](#)]
39. Li, X.; Chen, G.; Khan, F. Analysis of underwater gas release and dispersion behavior to assess subsea safety risk. *J. Hazard. Mater.* **2019**, *367*, 676–685. [[CrossRef](#)]
40. Li, X.; Chen, G.; Zhu, H.; Chang, Y. Study on release and dispersion behavior of underwater gas based on Eulerian-Lagrangian approach. *J. China Univ. Pet. (Ed. Nat. Sci.)* **2019**, *43*, 131–137.

41. Li, X.; Chen, G.; Zhu, H.; Xu, C. Gas dispersion and deflagration above sea from subsea release and its impact on offshore platform. *Ocean. Eng.* **2018**, *163*, 157–168. [[CrossRef](#)]
42. Xiong, J.; Cheng, R.; Lu, C.; Chai, X.; Liu, X.; Cheng, X. CFD simulation of swirling flow induced by twist vanes in a rod bundle. *Nucl. Eng. Des.* **2018**, *338*, 52–62. [[CrossRef](#)]
43. Liu, C.; Liao, Y.; Wang, S.; Li, Y. Quantifying leakage and dispersion behaviors for sub-sea natural gas pipelines. *Ocean. Eng.* **2020**, *216*, 108107. [[CrossRef](#)]

**Disclaimer/Publisher’s Note:** The statements, opinions and data contained in all publications are solely those of the individual author(s) and contributor(s) and not of MDPI and/or the editor(s). MDPI and/or the editor(s) disclaim responsibility for any injury to people or property resulting from any ideas, methods, instructions or products referred to in the content.